Development of Human Muscle Protein Measurement with MRI

Final Report

for

NASA Cooperative Agreement (NCC 9-36)

Round I Subcontract

August 15, 1997

Investigators:

Chen Lin, Ph.D.
Assistant Professor
Baylor College of Medicine

Harlan Evans, Ph.D.
Assistant Professor
Baylor College of Medicine

Adrian D. LeBlanc, Ph.D.
Professor
Baylor College of Medicine

1. INTRODUCTION

It is known that micro-gravity has a strong influence on the human musculoskeletal system. A number of studies have shown that significant changes in skeletal muscles occur in both space flight and bedrest simulation. In our 5 week bedrest study (1), the cross-sectional area of soleus-gastrocnemius decreased about 12% while the cross-sectional area of anterior calf muscles decreased about 4%. Using volume measurements, these losses increased after 17 weeks to approximately 30% and 21% respectively (2). Significant muscle atrophy was also found on the SL-J crew members after only 8 days in space (3). It is important that these effects are fully understood so that countermeasures can be developed. The same knowledge might also be useful in preventing muscle atrophy related to other medical problems.

A major problem with anatomical measurements of muscle during bed rest and microgravity is the influence of fluid shifts and water balance on the measurement of muscle volume, especially when the exposure duration is short and the atrophy is relatively small. Fluid shifts were documented in Skylab by visual observations of blood vessel distention, rapid changes in limb volume, center of mass measurements and subjective descriptions such as puffy faces and head fullness (4). It has been reported that the muscle water content of biopsied soleus muscles decreased following 8 hours of head down tilt bed rest (5). Three aspects of fluid shifts that can affect volume measurements are: first, the shift of fluid that occurs whenever there is a change from upright to a recumbent position and vice versa; second, the potential for fluid accumulation in the lower limbs resulting from muscle damage caused by overextending atrophied muscle or swelling caused by deconditioned precapillary sphincter muscles during reambulation (6); third, the net change of hydration level during and after bed rest or spaceflight.

Because of these transitory fluid shifts, muscle protein is expected to represent muscle capacity better than does muscle volume. The purpose of this study is to test the feasibility of using MRI to quantify of muscle protein and water content changes in muscle.

2. THEORETICAL APPROACH

The major components of muscle are muscle protein and water. Part of the water, the bound water, is associated with the protein and it is MRI "invisible". The remainder of the water is the unbounded water.

Under the physiological condition, skeletal muscle is well hydrated. The protein and water molecules are closely associated and the muscle volume, V_M, can be represented as the sum of the protein volume, V_P, the bound water volume, V_{BW}, and the unbound water volume, V_{UBW}.

$$V_M = V_P + V_{BW} + V_{UBW}$$

If one assumes that there is no significant composition and molecular conformation changes of the muscle protein as the result of atrophy, one would expect the ratio, *f*, between the amount of protein and the amount of the bound water to be constant because the interaction between the muscle protein and water remains the same.

$$V_{BW} = f * V_P$$

The unbound water volume in the muscle can be determined by MRI proton density measurement.

$$V_{UBW} = PD_M/PD_W * V_M$$

where PD_M is the measured proton density of the muscle and PD_W is the proton density of bulk water such as a water phantom.

V_P, the protein volume within the muscle, is directly related to the number of protein molecules or the protein mass.

$$M_P = D_P * V_P$$

where D_P is the average density of muscle protein when closely packed.

Combining all the equations above, we have:

$$M_P = D_P/(1+f)\,(1 - PD_M/PD_W)\,V_M$$

The MRI images acquired at different TE's may be used to generate proton density images of muscle and to measure PD_M/PD_W. Muscle volume, V_M, can also be measured from these images. $D_P/(1+f)$ is a constant. For measuring relative changes, the exact value of $D_P/(1+f)$ is not important. To make absolute measurements, the constant factor $D_P/(1+f)$ will can be determined through other experimental methods. One possible method is to dry and weight animal muscle samples after the MRI measurement.

3. METHODS

3.1 Proton Density Measurement and Image Intensity Correction

The key step in this experiment is to make accurate measurement of the relative muscle proton density, PD_M/PD_W. Theoretically, the signal intensity in the MR image is proportional to the proton density. However, several factors will cause the deviation from this ideal situation (7).

First, the radio frequency excitation pulse sent out by the transmitter coil has a non-uniform distribution. This will cause the degree of excitation to vary within the region of interest. Second, the receiver coil has a different sensitivity at the different signal source locations. Therefore, the scaling factor between the proton density and measured image intensity varies across the image. This is known as the sensitivity profile.

The sensitivity profile also varies with time. The tunings of coils, the transmitter and the receiver of an MRI scanner are adjusted for each subject. The result of adjustment could be different each time even for the same subject. The variation in positioning of the subject will also cause the coupling between the subject and coil to be different. All of these will cause the sensitivity profile to vary from one MRI measurement to another.

3.1.1 Design and Construction of phantoms

To correct for the spatial and time variations, we performed scans on uniform phantoms to measure the sensitivity profile of the MR scanner with the body coil as both transmitter and receiver. These scans were used to calibrate the in-vivo calf measurement.

Two sets of phantoms were constructed to obtain the image intensity correction (See Appendix A). One set of phantoms consisted of six plexi-glass tubes filled with $MnCl_2$ doped distilled water. They were mounted on a frame surrounding the imaging volume intended for imaging the calves of subjects. Another set of phantoms was two large plexi-glass cylinders filled with corn oil. They are large enough to cover the imaging volume for the subject's calves.

To measure the sensitivity profile, the six water phantoms and the two corn oil phantoms were imaged together in a configuration shown in the appendix B. Additional coil loading phantoms were also included to simulate the human upper body when the phantom images were taken so that the coil is adjusted under similar conditions.

The image intensities from the water phantoms provides the information of the offset (zero order coefficient) and gradients (first order coefficients) in the sensitivity profile. The higher order variation can be estimated by comparing the image intensities in the oil and the water phantoms as shown in the next section. The water phantoms will also be included in the in-vivo measurement of calves. Again, this allows us to estimate the linear variations in the sensitivity profile for the actual calf measurement. We combined the linear term measured with the calves and the higher order term measured from the phantoms to correct for the sensitivity variation. This approach allows us to compensate for the linear changes in the sensitivity profile when the scanner re-adjusts between phantoms and calves.

The reason for using corn oil instead of water is because the di-electric constant of corn oil is similar to that of muscles. The di-electric constant of water is much larger and thus causes significant RF attenuation towards the center of large uniform water phantoms.

3.1.2 Phantom scan

The calibration measurements were made on a Siemens 1.5T Magnetom SP imager at The Methodist Hospital. A double-echo spin-echo sequence, SE_20B130_45B130.UDB, was used to image the calibration phantoms assembled in the configuration described previously. The SE_20B130_45B130.UDB sequence produces two images at echo-times of 20ms and 45ms for each of the 32 consecutive 10mm slices over the entire length of the phantoms. This is the same protocol used for the calf measurement. Measuring image intensities at multiple echo times is necessary for calculating T2 and extrapolating the data back to time zero for proton density measurement. Although a more precise way of determining T2 employs a single-echo sequence, acquiring images at more than two echo times, such an approach is time consuming and therefore not practical for in-vivo study. The field of view was 300mm and the matrix size was 256 x 512 with the rectangular option. The built-in body coil was used for both RF transmission and reception. Figure 1 shows a typical cross-sectional image of the calibration phantoms.

Figure 1. Transverse image of sensitivity calibration phantoms

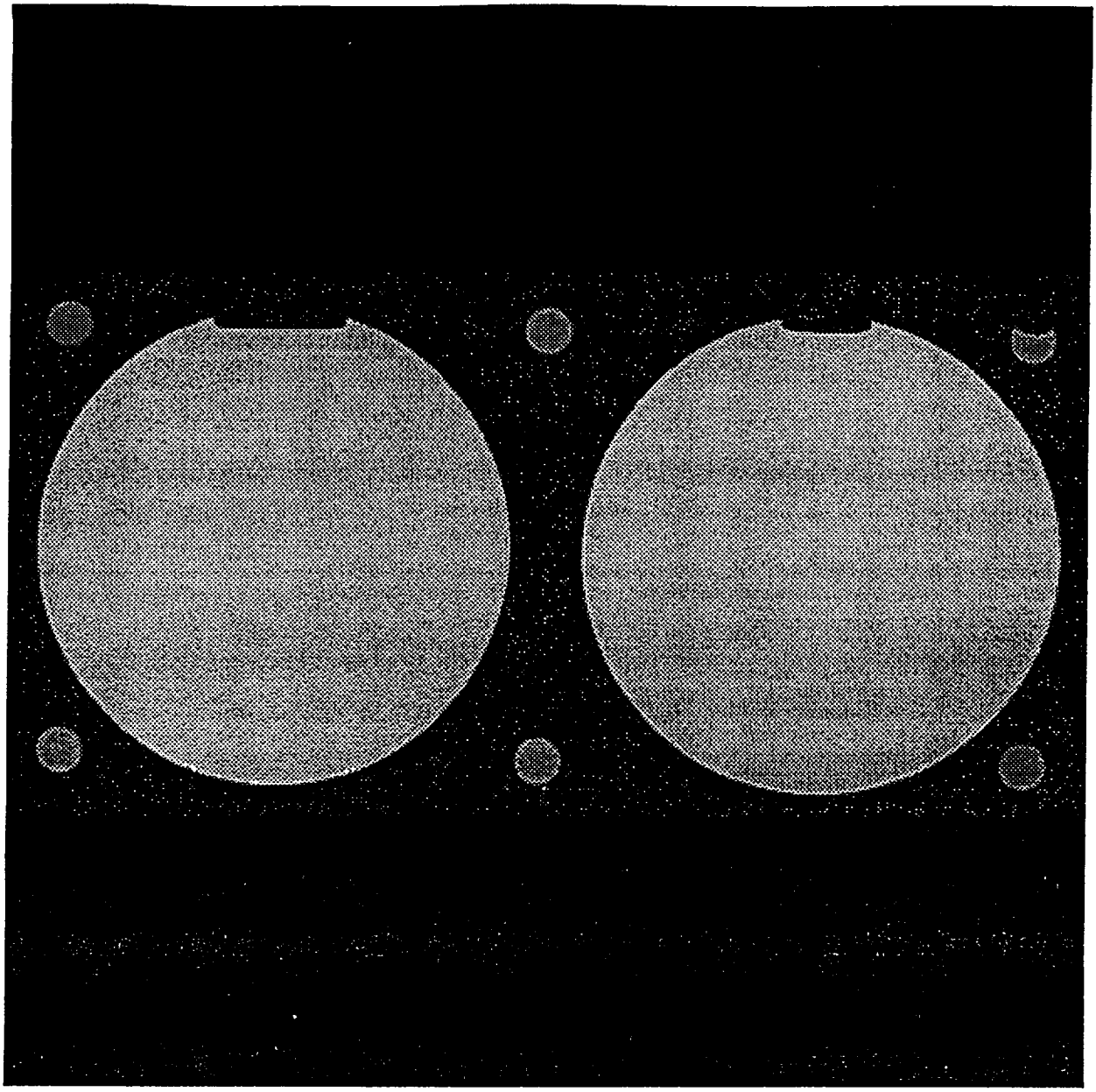

3.1.3 Measuring Sensitivity Profile from Phantom Images

The first step is to extract linear correction images and the high order correction image from the phantom images. This procedure for this is shown in the following flow chart.

Figure 2. Flow chart of sensitivity correction procedure

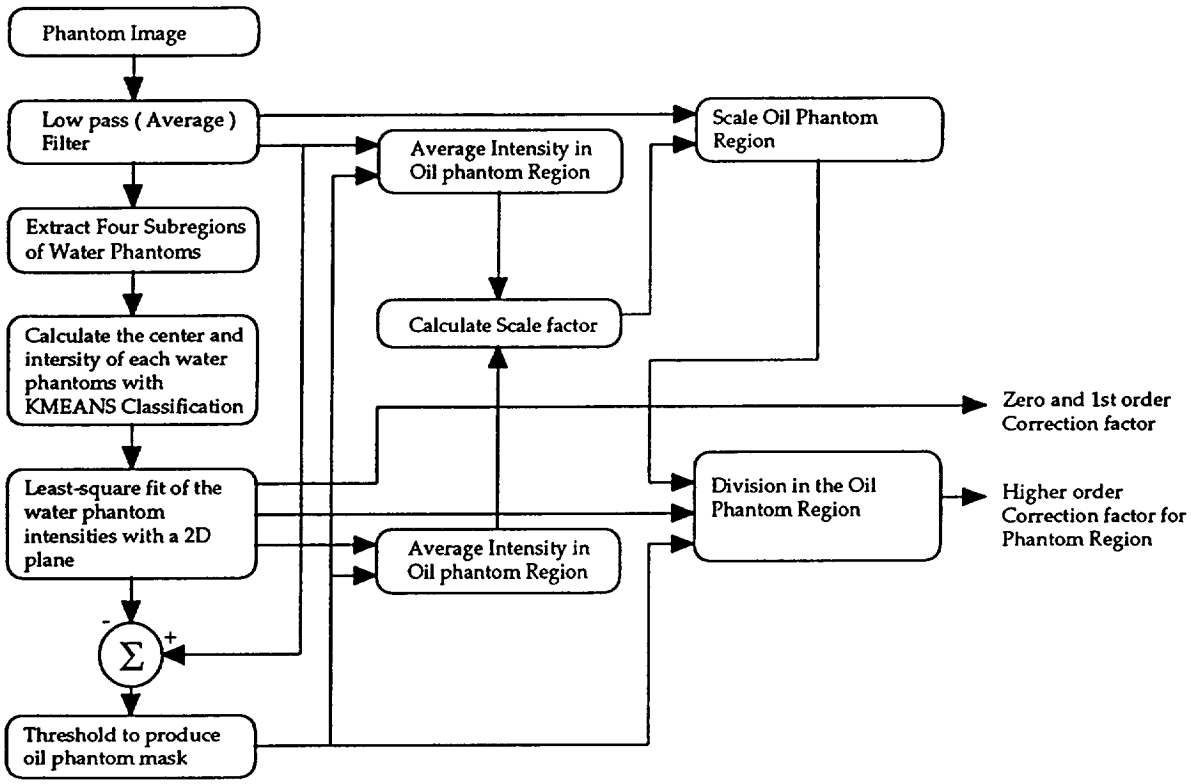

A 3x3 average filter is first applied to the phantom images to reduce the noise. The image is then separated into two parts each containing a large corn oil phantom and four small water phantoms. The two parts are treated separately in the following processing.

Four small regions each including a water phantom were extracted. For each region a Khoros KMEANS routine is used to calculate the average intensity and the center of the water phantom. The average intensities and the center coordinates of the four water phantoms were analyzed with a least-square fitting routine to define a tilted plane which represents the linear sensitivity variation.

After subtracting the linear sensitivity variation from the original images, the image intensity in

the corn oil phantom region was still not constant because of the higher order terms in the sensitivity variation. The following two histograms show the image intensity variation in the oil phantom region before and after subtracting the linear term. After the correction, the peaks in the histogram is much narrower which means the linear term had a significant contribution to image intensity correction.

Figure 3. The histograms of oil phantom before and after correction

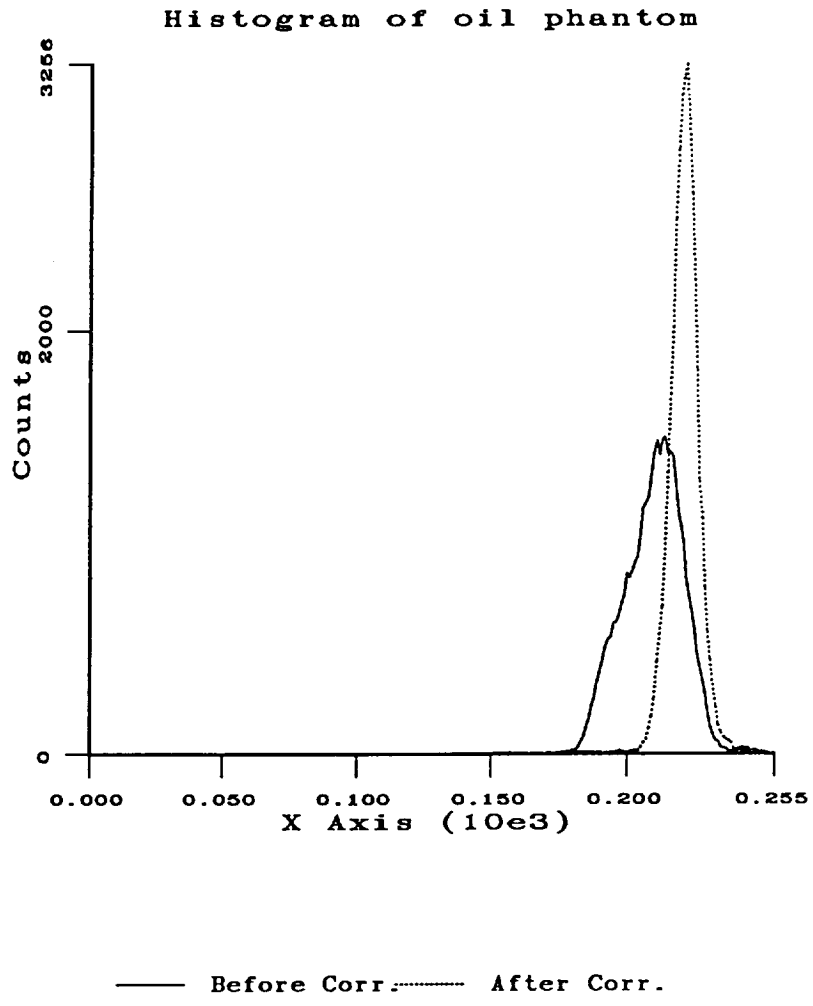

The higher order term characterized by the inhomogenity in the oil phantom region can not be used directly for image intensity correction because the signal intensity is different between oil

and water. The image intensity in the corn oil phantom region must be scaled to the image intensity of water before it can be used for higher order correction. The scaling factor was calculated in the following way. First, a mask for the corn oil phantom region was determined using an appropriate threshold after the linear sensitivity variation was removed from the original image. An erosion operation on the mask removed edge pixels. Using this mask, the average image intensity for the oil phantom region was calculated from both the original image and the linear correction image. The ratio between these two averages was used as the scale factor for the oil phantom region.

After scaling down the image intensity in the oil phantom region to correspond with water phantom and subtracting the linear correction, the remaining inhomogeneity represents the higher order terms in the sensitivity variation.

The image processing steps described above were done on Sun Unix workstations using routines in Khoros image processing software and programs developed in C language.

3.1.4 Calf scan

Calf scans were done on the same MRI system with the same protocol as the phantom scans described above. Both calves were positioned in place of the oil phantoms and surrounded by six water phantoms mounted on the frame. The locations of the 32 slices were also kept the same as in the phantom scan. This is to ensure a one to one correspondence between the phantom images and calf images. The sensitivity profile measured from the corresponding phantom image can be used directly to correct the calf image without further interpretation for slice position difference. A typical calf image is shown in following figure 4.

Figure 4. Transverse image of human calf

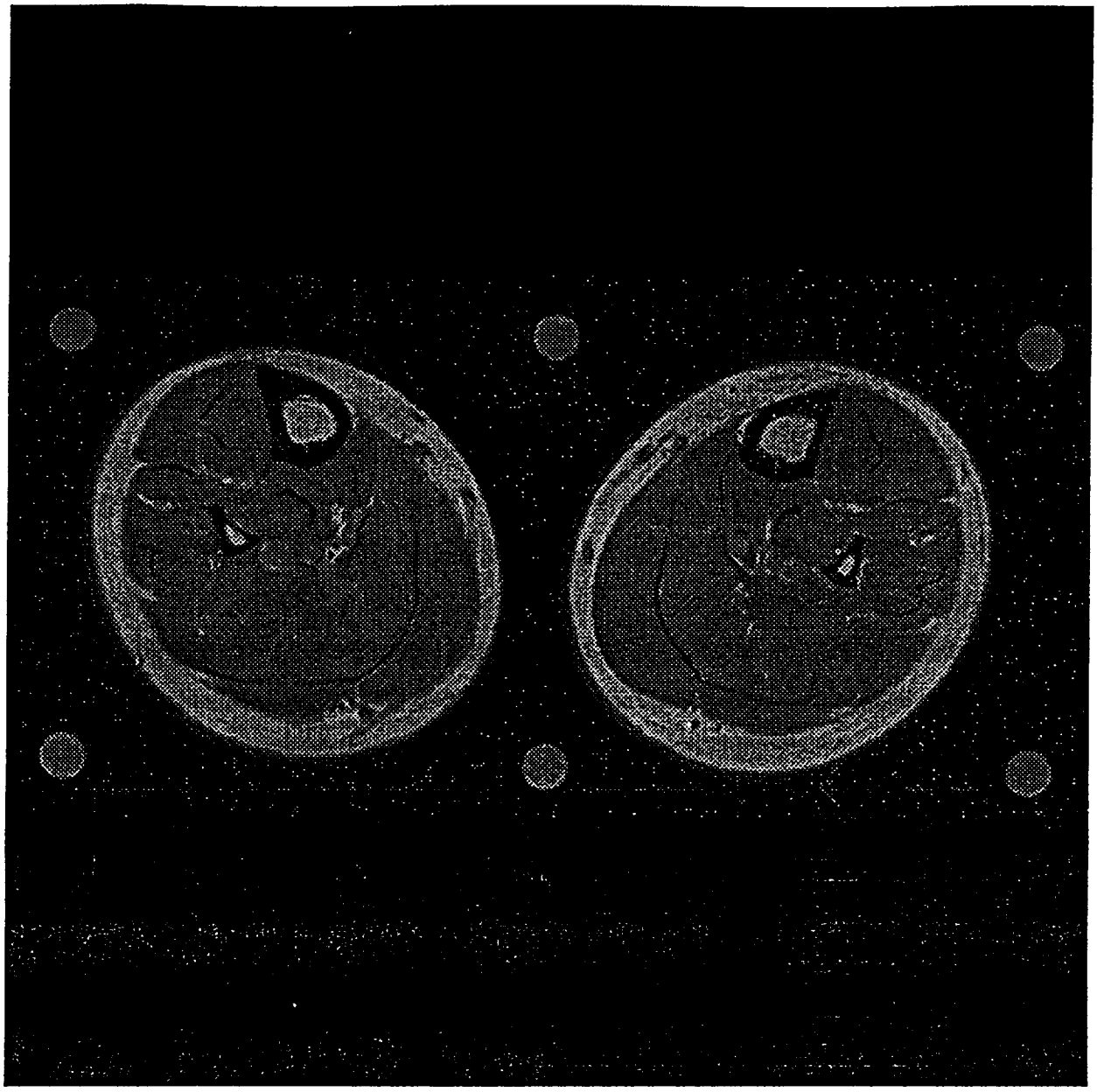

From each half of the calf image, the linear sensitivity variation was measured from the image intensity of water phantoms at the four corners. The same algorithm used for phantom images was applied here. Using both the linear sensitivity variation measured from calf images and the higher order sensitivity variation measured from the corresponding phantom images, the calf image intensity was corrected and calibrated relative to water.

3.1.5 Results of calf sensitivity profile measurement and correction

Successful image intensity corrections by using a uniform phantom as reference have been reported in the literature (8,9,10). These corrections were based on the assumption that the image intensity variations are mainly determined by the geometry of the MRI coil and, therefore, the variation does not change significantly between the subject and the phantom. However, the purpose of these corrections are mainly for image display or image segmentation. For quantitative proton density measurement, a more accurate image intensity is required. Our technique attempts to accomplish this. In our techniques, the sensitivity profile difference between the phantom images and calf images is compensated up to first order.

However, the result of our study shows our technique was not effective in correcting calf images. There was no dramatic improvement in calf image uniformity before and after correction. No significant difference was found in the calf image histograms before and after the calf image intensity correction. The width of muscle and fat peaks in the histograms remained the same.

The main reason for the poor performance of our techniques was that the pattern of image intensity variations in the calf images was dramatically different from the pattern in the corn oil phantom images. Even though the oil phantoms were constructed to have similar dimensions of human calf, there was no significant correlation in the sensitivity profile between calf and phantom images. In this case, the uniform phantom based technique is invalid. Our technique is only as good as a linear correction. Such a large and unexpected image intensity difference has not been reported. The cause for this difference is still under investigation.

A new algorithm which does not require using a uniform phantom to measure the sensitivity profile is currently under development. This algorithm divides the image into many small regions. In each region, image intensity variation is relatively small and, therefore, the fat and muscle component can be easily separated. Assuming that the image intensity for all the muscle

pixels are the same, a correction mask can be created by comparing the average muscle pixel intensity difference between each small region. Preliminary study shows that this algorithm may produce better results than the uniform phantom based approach. This technique may be used to replace the uniform phantom technique for the sensitivity correction, therefore, allowing accurate proton density measurement over a large region of interest.

3.2 In-vitro test of T2 & PD sensitivity to protein concentration

In order to test the sensitivity and accuracy of our technique, we attempted to measure the water content in a set of phantoms in which the protein concentration and water content were accurately known.

3.2.1 Protein phantom preparation

The major components of muscle fiber are actin and myosin. Ideally, the phantoms should be constructed using solutions of actin and myosin with known concentrations to mimic muscle. Since these proteins are very expensive, we have elected to use other macromolecules which are similar in molecular structure to actin and myosin.

We initially tested gelatin and found that it does not produce uniform solutions for the concentrations similar to protein concentration of muscle. We finally chose Polypep (11), a mixture of polypeptides with various chain lengths, from Sigma Chemicals. It forms stable solution or gels for a wide range of concentrations.

Four protein phantoms were constructed by dissolving Polypep in distilled water doped with 0.5mM magnesium chloride. A phantom of doped water without any Polypep was included as reference. The amount of water and Polypep in each phantom are listed in Table 1. There are three phantoms with high concentration of protein. Those concentrations are similar to the protein concentration in muscle. The correct amount of water and Polypep were weighted with a precision balance and mixed in a small vial. The sealed vial was then placed in a 60C water bath and shaken periodically until uniform solution or gel was formed.

3.2.2 Protein phantom measurement

Protein phantoms are scanned with the same double-echo imaging sequence with echo times of 20ms and 45ms. Single-echo spin-echo sequence, SE_10B130.UDB, was also used to acquire

images at echo times' 10ms, 30ms, 50ms, 70ms and 90ms. The measurement with the single echo sequence provides a more accurate measurement of the decay curve. The standard Siemens head coil was used instead of the body coil for better signal to noise ratio. Also a smaller field of view of 150mm and matrix size of 256 x 256 was used. A single 10mm thick slice was acquired at each TE.

All protein phantom measurements were done at room temperature. Certain MRI parameters, such as relaxation time and the "MRI visible" protons, will have slightly different values at room and body temperature. However, since the main purpose of this experiment was to test the sensitivity instead of calibrating the absolute value, these differences were acceptable.

Transverse relaxation time (T2) and proton density images of the phantoms were generated by least square fitting of the images at different echo times. The proton density and relaxation time measured with single echo and multiple echo sequences did not differ significantly.

The volume of the phantom is different from the volume of water after the Polypep is dissolved. The final volume of each protein phantom can not be calculated easily and therefore were measured using the MRI images. The phantom image of the first echo was thresholded to separate the phantom image from the background. The height of each phantom was measured by counting the pixels. The height of each phantom was used to calculate its volume.

3.2.3 Protein phantom results

The images of a set of protein phantoms in a water bath are shown below in figure 5. Imaging the phantoms in a water bath is necessary because of the coil sensitivity profile is not uniform. Even for a small field of view inside a head coil, there is a significant change of sensitivity over the images. The sensitivity variation was mostly along the axis of the magnet or the coil. This variation can be measured from the water bath image and in shown in figure 6.

Figure 5. MRI image of protein phantoms

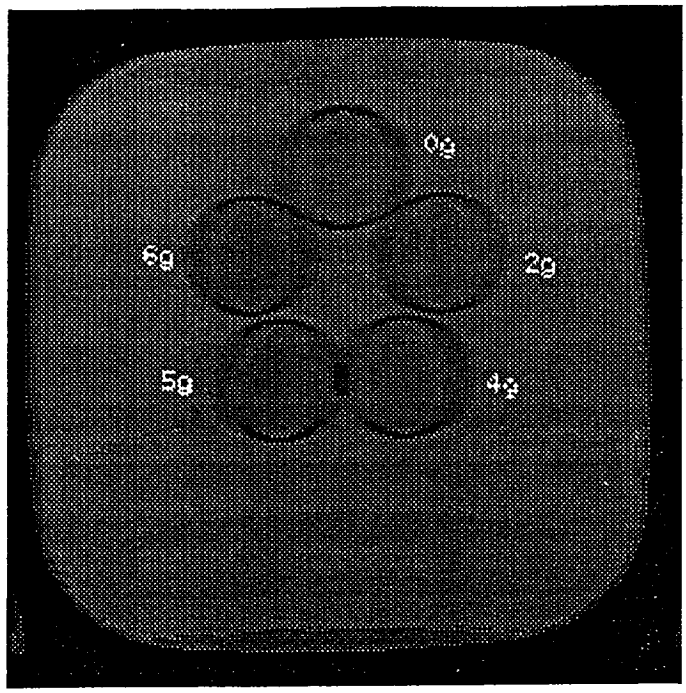

Figure 6. Sensitivity profile of Siemens head coil

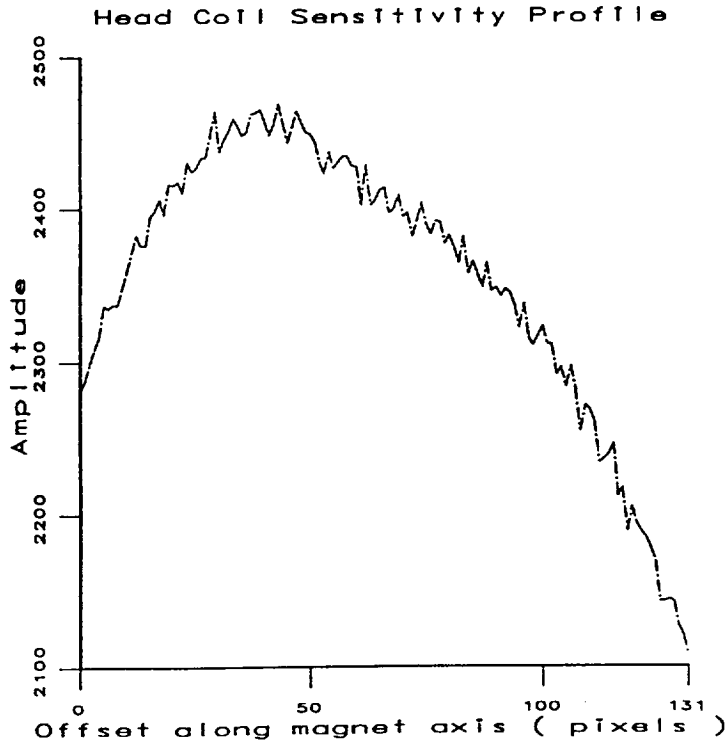

The results of the MRI measurements of protein phantoms is summarized in the following table:

Table 1. MRI results of Polypep phantoms in a water bath

Phantom Number	1	2	3	4	5
Polypep (gram)	0.00	2.00	4.00	5.00	5.99
H_2O (gram)	20.00	18.02	16.02	15.05	14.00
Phantom Height (pixels)	49	48	47	46.5	45
Phantom Volume (Calculated in ml)	20.0	19.6	19.2	19.0	18.4
Proton Density (Calculated, relative to water)	1	0.92	0.83	0.79	0.76
Image Intensity of Polypep Phantoms	2852	2807	2590	2575	2737
Image Intensity of Water Bath	2869	2862	2710	2710	2862
Proton Density (Measured, relative to water)	1	0.98	0.96	0.95	0.95
T2 (msec)	28.8±0.5	30.1±0.5	25.7±1.0	25.2±0.6	23.9±0.5

The height of Polypep phantoms was calculated from the MRI image. Since the liquid volume of the 20 grams water phantom is 20 ml and the diameter of all the glass vials used for these phantoms are the same, the volumes of the other Polypep phantoms can be estimated from their height relative to the one which has only water. Using calculated volumes and amount of water in the phantom, one can calculate the proton density. The calculated proton density is listed relative to water proton density. The three Polypep phantoms with high protein concentrations had calculated proton densities ranging from 76% - 83%. The water content of normal human muscle is within this range.

The transverse relaxation, T2, of the three phantoms with high protein concentration ranges from

24 msec to 25 msec. These T2 values are also very similar to that of human muscles which is typically between 20 msec to 30 sec.

The calculated water content, the T2 value and the gel-like physical appearance suggest than these protein phantoms resemble human muscle. However, the measured proton densities were different from the calculated proton densities. The dependence of measured proton density on Polypep content is also much weaker than expected.

3.2.4 Proton spectroscopy of Polypep phantom

As discussed above, the proton density measured by MRI differs dramatically from the calculated value. One possible reason is that the signal from protons on the Polypep is actually "MRI visible". The signal from protons may be included in the images causing the measured proton density to be higher than the expected value. Most protons on Polypep should be in CH_2 group. The frequency of signals from CH_2 protons is slightly different from the frequency of water protons. If the Polypep protons are "MRI visible", there will be a second peak in addition to the water peak in the proton spectrum. Volume localized spectroscopy was therefore performed on one of the phantoms to verify its composition and to measure the T2 independently.

Figure 7 Proton spectrum of Polypep phantom

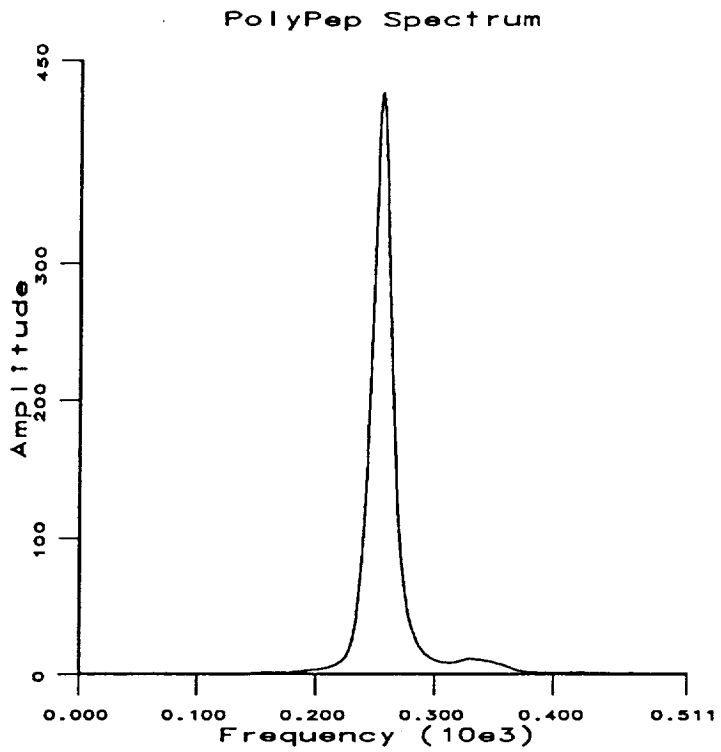

The spectrum of a Polypep phantom does show two peaks. The large one corresponds to the water signal and the small peak corresponds to CH_2 protons on the chains of Polypep. Their ratio is 15:1 This is an expected ratio because most of the phantom is water and only a few of the protons on the mobile side chain of Polypep can be detected. It does not account for the greater than expected proton density in Polypep phantoms. The T2 of both peaks in the spectrum was 27.0 msec, which agrees with the T2 measured on spin echo images.

3.2.5 Analysis of protein phantom results

The only possible explanation the protein phantom experiment results is that the protons on Polypep molecule are contributing to the proton signal measured by MRI. This would require that the protons on Polypep chain to be fairly mobile. There could be two mechanisms for the Polypep protons to have large mobility. One reason is that the Polypep chain itself is very dynamic. The motion of Polypep chain is much greater than expected. The other reason is that the protons on Polypep molecules are loosely bonded. They are constantly exchanging with

protons in the solution. Both mechanisms are unlikely for a large peptide chain such as the Polypep and the spectroscopy result rules out the first reason. Further studies will be performed to investigate this problem.

4. RESULTS AND DISCUSSION

An improved MRI image intensity correction and calibration technique has been developed for proton density measurement over a large region. This technique uses two sets of water and corn coil phantoms to measure the sensitivity profile for both the phantom scan and the actual scan. By comparing the image pixel intensity in the phantom region, the pixel intensity in the actual scan region can be corrected and calibrated against the water value. This two-step image intensity calibration technique can compensate for the limited sensitivity profile change when the scanner readjusts between uniform phantoms and human calves, therefore, allowing more precise measurement of proton density over the conventional uniform phantom technique.

Our experiment shows there is a large, unexpected sensitivity profile change between imaging the uniform phantoms and the calves. Such a large difference has not been reported previously. Further investigations are needed to identify the source of this difference. A more robust technique of image intensity correction is under development which may provide the solution to this problem.

Our Polypep phantom experiment indicates that the proton density is not sensitive to the amount of Polypep in our protein phantom. As shown in table 1, the amount of water in each phantom is significantly different and the final volume of the solution or gel is about the same after the Polypep is dissolved. This suggests that protons on the Polypep itself are also contributing to the MRI signal so that the total proton density is about the same. This is an different than what is generally believed that the protons on the macromolecules are MRI "invisible". Therefore, Polypep may not be suitable for testing our technique. At this point, we are unable to find a good model which will allow us to test this technique in vitro.

5. REFERENCES

1. LeBlanc A.; Gogia P.; Schneider V.; Krebs J.; Schonfeld E.; Jhingran S.; and Johnson P. Calf Muscle Area and Strength Changes After Five Weeks of Horizontal Bed Rest. Am. J. of Sports Medicine 16:624-629, 1988.

2. LeBlanc A.D.; Schneider V.S.; Evans H.J.; Pientok C.; Rowe R.; and Spector E. Regional Changes in Muscle Mass Following 17 Weeks of Bed Rest. J. Appl. Physiol. 73(5):2172-2178, 1992.

3. LeBlanc A.D.; Rowe R.; Schneider V.S.; Evans H.J.; and Hedrick T.D. Regional Muscle Loss After Short Duration Space Flight. Aviation, Space and Enviromental Medicine, In Press

4. Thornton W.E.; Hoffler G.W.; and Rummel J.A. Anthropometric Changes and Fluid Shifts. In: Dietlein, L. (Ed). Biomedical Results from Skylab. U.S. Govt. Printing Office, Washington, D.C., pp. 330-338, 1977.

5. Typton C.M.; Hargens A.R.; Gollnick P.D.; Mubarak S.J.; Gonsalves M.R.S.; and Tucker B.J. Influence of Head-Down Tilt on Muscle to Action and Starting Forces. American College of Sports Medicine (abstract), 1980.

6. Hargens A.R. Fluid Shifts in Vascular and Extravascular Spaces During and After Simulated Weightlessness. Med. Sci. Sports Exerc., 15(5):421-427, 1983.

7. A. Simmons, P. S. Tofts, G. J. Baker and S. R. Arridge Source of Intensity Nonuniformity in Spin Echo Images at 1.5T Magn. Reson. Med. 32:121-128, 1994

8. G. Brix, L. R. Schad and W. J. Lorenz Evaluation of Proton Density by Magnetic Resonance Imaging: Phnatom Experiments and Analysis of Multiple Component Proton Transverse Relaxation Phys. Med. Biol. 35(1)53-66 1990

9. D. A. G. Wicks, G. J. Barker and P. S. Tofts Correction of Intensity Nonuniformity in MR Images of Any Orientation Magn. Reson. Imaging 11:183-196 1993

10. P. S. Tofts, G. J. barker, A. Simmons, D. G. MacManus, J. Thrope, A. Gass and D. H. Miller Correction of Nonuniformity in Images of the Spine and Optic Nerve from Fixed Receiver-only Surface Coil at 1.5T J. Comput. Assist. Tomogr. 18(6)997-1003 1994.

11. Product Index, Sigma Chemical Company St. Louis, MO 63178

6. APPENDIX

Appendix A

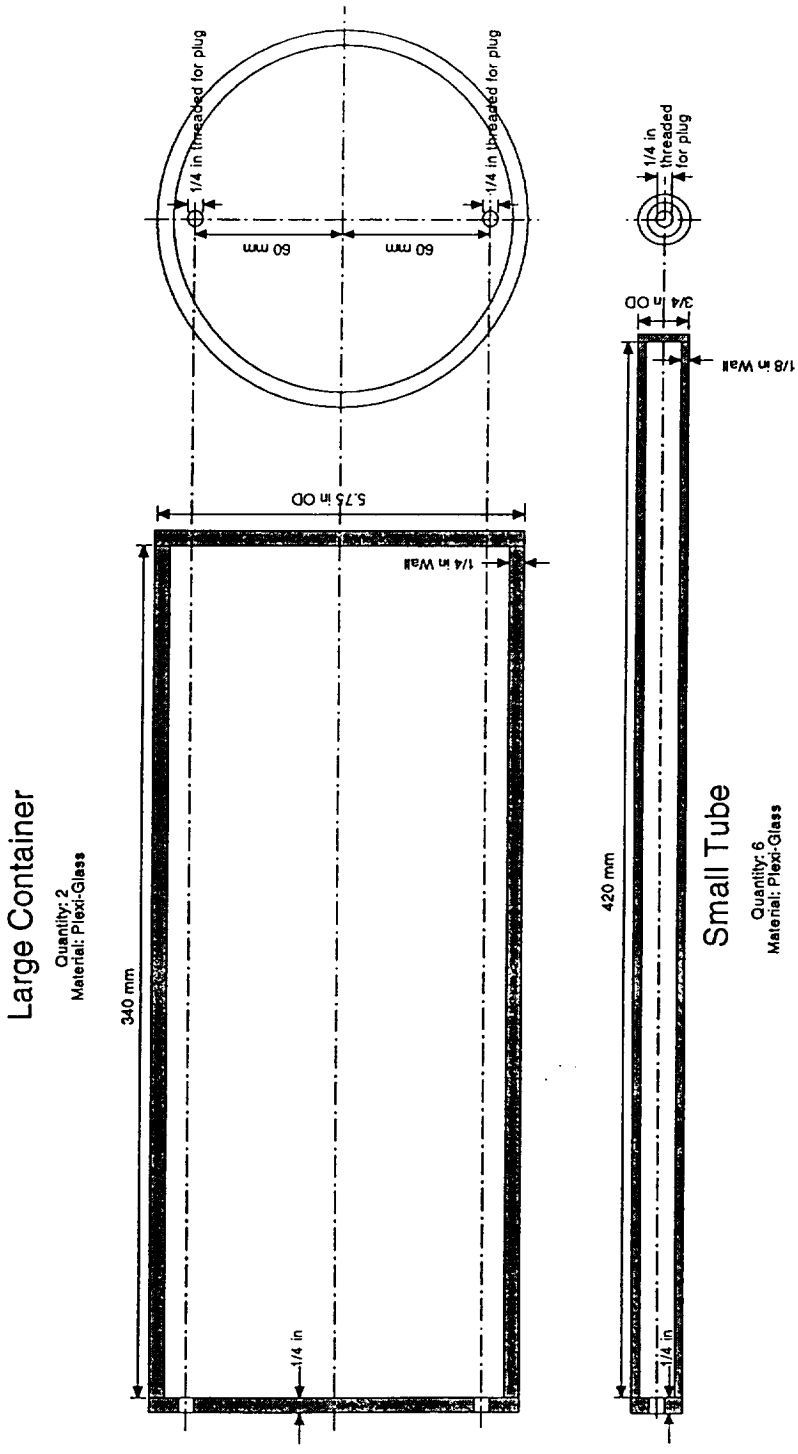

Appendix B

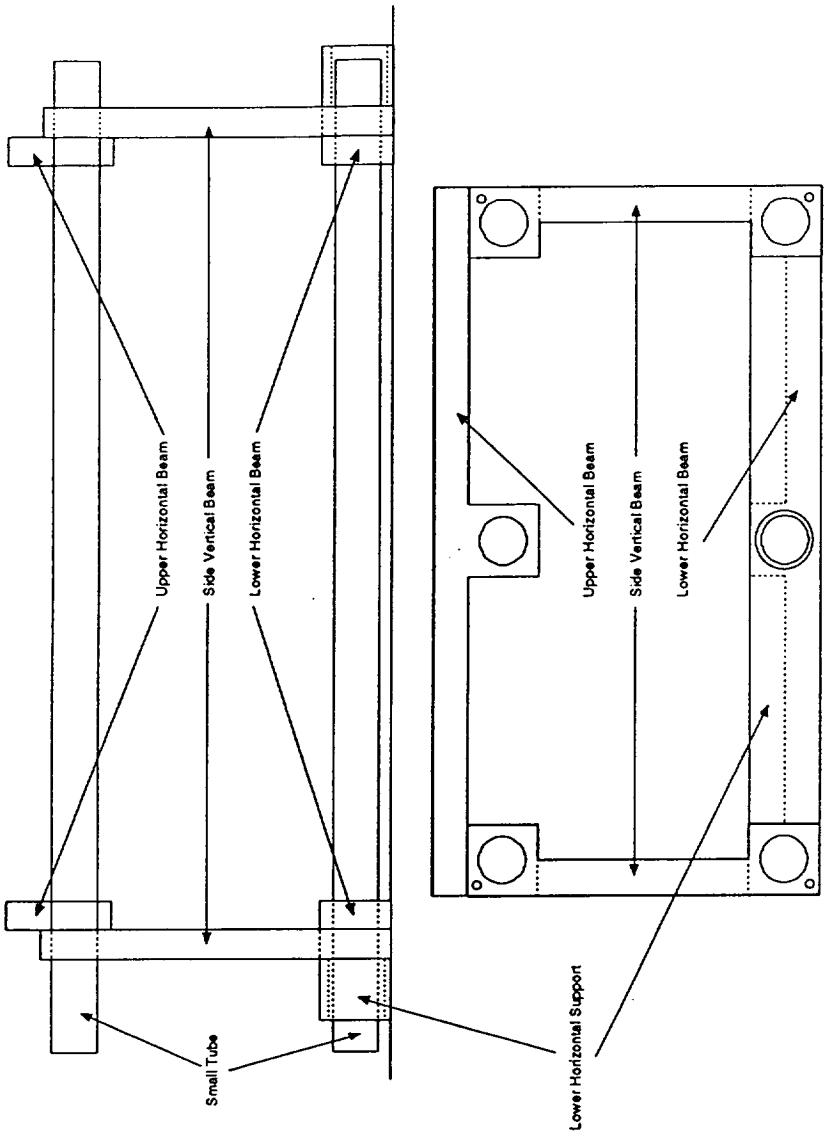
Upper Horizontal Beam
Side Vertical Beam
Lower Horizontal Beam
Small Tube
Lower Horizontal Support
Upper Horizontal Beam
Side Vertical Beam
Lower Horizontal Beam